ISSN 0022-4766, Journal of Structural Chemistry, 2024, Vol. 65, No. 4, pp. 643-654. © Pleiades Publishing, Ltd., 2024.
Russian Text © The Author(s), 2024, published in Zhurnal Strukturnoi Khimii, 2024, Vol. 65, No. 4, 124527.

COVALENT FUNCTIONALIZATION OF FEW-LAYER BLACK PHOSPHORUS BY THE COMPLEX [$NiBr_2$(phen)] (phen = 1,10-PHENANTHROLINE)

Aidar M. Kuchkaev[1]*, Airat M. Kuchkaev[1], A. V. Sukhov[1,2], S. V. Saparina[3], O. I. Gnezdilov[3], A. E. Klimovitskii[2], S. A. Ziganshina[4], I. R. Nizameev[1], B. A. Faizullin[1], O. G. Sinyashin[1], and D. G. Yakhvarov[1]**

A 2D material few-layer black phosphorus (FLBP) has promising applications in various fields of chemistry and physics due to its unique electronic and optical properties. Chemical functionalization of the FLBP surface is an effective strategy for improving the oxidative stability of the material, tuning its intrinsic properties or endowing it with new properties. The present work proposes an approach to the immobilization of the [$NiBr_2$(phen)] complex (phen = 1, 10-phenanthroline) on the FLBP surface via covalent functionalization of FLBP with 1,10-phenanthroline and subsequent complexation with $NiBr_2$. The obtained FLBP-based materials functionalized by the [$NiBr_2$(phen)] complex were characterized by a set of physicochemical methods such as transmission electron microscopy, atomic force microscopy, solid-state NMR, energy-dispersive spectroscopy, Raman spectroscopy, and IR spectroscopy.

DOI: 10.1134/S0022476624040012

Keywords: black phosphorus, phosphorene, covalent functionalization, diimine ligands, 1,10-phenanthroline, nickel complexes, diazo compounds.

This work was reported at the 4th Russian Conference "Graphene: molecule and 2D crystal"

INTRODUCTION

In the past decade, the physics and chemistry of 2D materials based on black phosphorus (BP) has witnessed rapid development. After the BP-based 2D structures such as the few-layer black phosphorus (FLBP) and phosphorene (phosphorus analogue of graphene) were prepared, there has been much work to study the physical and physico-chemical

[1]Arbuzov Institute of Organic and Physical Chemistry, Kazan Scientific Center, Russian Academy of Sciences, Kazan, Russia; *kuchkaev95@mail.ru, **yakhvar@iopc.ru. [2]Butlerov Institute of Chemistry, Kazan Federal University, Kazan, Russia. [3]Institute of Physics, Kazan Federal University, Kazan, Russia. [4]Zavoisky Physical-Technical Institute, Kazan Scientific Center, Russian Academy of Sciences, Kazan, Russia. Original article submitted November 8, 2023; revised December 5, 2023; accepted December 7, 2023.

properties of this material and to create various FLBP-based devices [1]. Unusual puckered and highly anisotropic structure of FLBP, its unique semiconductor properties, high charge carrier mobility, and good biocompatibility make this material promising for applications such as electro- and photocatalysts, lithium- and sodium-ion batteries, field-effect transistors, lasers, solar cells, biomedical materials, etc. [2-5].

Covalent functionalization and modification of the FLBP structure can significantly improve its rather low oxidation stability, promote the impartment of new properties of the material, thus expanding the scope of its application [6-8]. Covalent functionalization of FLBP with organic substrates is most often achieved using highly reactive intermediates. FLBP can be functionalized with aryl radicals using the decomposition of the corresponding diazonium or iodonium salts [9, 10], free alkyl radicals [11, 12], carbenes [13], and nitrenes [14, 15] (Fig. 1). However, despite first significant successes, this direction is still at an early stage of development and requires additional research using new reagents and the development of new methods for FLBP functionalization.

The most common among the above methods is the diazonium chemistry, the most universal tool for covalent FLBP functionalization with various organic substrates, including those characterized by a complex structure [7]. Thus, diazonium chemistry was used to functionalize FLBP with Nile blue [16] and tetraphenylporphyrin [17]. As a result of functionalization, FLBP acquired new optical and photophysical properties, thus expanding the scope of its possible applications. Moreover, this method can be also used to prepare materials bearing new functional groups. For example, FLBP functionalized with 4-bromomethyl groups was used as a cross-coupling reagent for the chemical cross-linking of a polymer bearing alkyne fragments using the Sonogashira reaction [18].

In general, virtually any aryl fragment can be attached to the FLBP surface, provided that the corresponding diazonium salt is stable. In terms of preparing new FLBP-based functional materials, it is highly interesting to use the diazonium chemistry to functionalize FLBP with various organic ligands and subsequent immobilization of transition metal complexes on the surface of this material. In particular, this approach can be utilized for the heterogenization of metal complexes exhibiting catalytic activity in various processes, for the conversion of a homogeneous process into a heterogeneous state in order to regenerate the employed catalyst. In this regard, nickel(II) complexes with diimine ligands were chosen as model objects for this study, since they exhibit high catalytic activity in the reaction of homogeneous oligomerization of ethylene and are currently quite well studied by various authors, including our team [19-21]. 1,10-Phenanthroline (phen) was chosen from diimine ligands for the FLBP functionalization, since this compound can be relatively easily converted to the diazonium salt from the corresponding amino derivative.

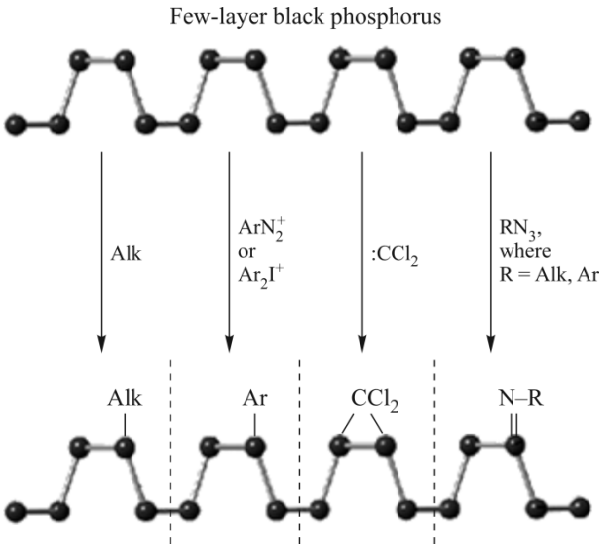

Fig. 1. Methods of FLBP functionalization by organic substrates.

Thus, the present work considers the possibility of using diazonium chemistry for the covalent functionalization of FLBP by 1,10-phenanthroline to immobilize the [$NiBr_2$(phen)] complex on the surface of a phosphorus 2D material.

EXPERIMENTAL

Physico-chemical methods

The transmission electron microscopy (TEM) images of FLBP particles were recorded on a Hitachi HT7700 (Japan) transmission electron microscope at an accelerating voltage of 100 kV. The samples were deposited on a 300 copper mesh with a Lacey carbon film (Agar Scientific). The energy-dispersive X-ray spectroscopy (EDS) experiments were conducted inside a TEM column operating at an accelerating voltage of 300 kV, where the sample was tilted by 15° to increase the EDS signal. The EDS spectra were obtained during a 10-second electron beam exposure.

The surface morphology of FLBP particles was studied in air by atomic force microscopy (AFM) in semi-contact mode on a Titanium microscope (NT-MDT, Russia) using a standard NSG-01 silicon cantilever (NT-MDT, Russia) with a resonant vibration frequency of 120 kHz. The substrate was a monocrystalline silicon plate containing silicon dioxide on its surface. The sample was prepared by a dropwise deposition of a suspension (5 μL) of the studied particles in acetonitrile and drying it in a vacuum.

The IR spectra were registered in the region of 4000-500 cm^{-1} with a resolution of 2 cm^{-1} on a Bruker Vertex 70 FTIR spectrometer equipped with a PIKE MIRacle single reflection ZnSe ATR unit. The background spectra obtained by 64 scans with a resolution of 2 cm^{-1} were subtracted from the spectra of the samples.

The Raman spectra were registered on a Bruker SENTERRA spectrometer using linearly polarized 532 nm light. The laser beam was focused on the sample surface using a 100x objective with a numerical aperture of 0.9 (configuration 180°). The laser power in spectroscopic experiments was 2 mW. The exposure time was 60 s. The Raman spectra were registered in the 45-3700 cm^{-1} range with a resolution of 3-5 cm^{-1}.

The UV-Vis absorption spectra were recorded on a Specord 50 Plus spectrophotometer (Analytik Jena AG, Germany) in 10 mm quartz cuvettes.

The ^{31}P MAS NMR spectra were recorded on a Bruker NMR AVANCE 400 WB spectrometer at 293 K. The measurements were carried out on ^{31}P phosphorus nuclei at a frequency of 162.056 MHz using a MAS 4 BL CP BB DVT sensor. The studied samples were placed in a 4 mm zirconium oxide rotor. The samples were rotated at a magic angle at a rate of 12 kHz. The duration of exciting 90-degree pulses for phosphorus nuclei was 3.4 μs. The spectra were recorded using standard pulse programs zg, hpdec, and cp. The total number of scanned points was 2048 (in all experiments), the number of scans in the FID trace varied from 256 to 512 to obtain an acceptable signal-to-noise ratio. The time between FID accumulations in the experiments on phosphorus nuclei was 20 s. The width of the obtained spectra was 69.5 kHz. The time in cross-polarization experiments varied from 1 ms to 5 ms to obtain the maximum signal.

The ^{1}H NMR spectra were registered on a Bruker Avance III spectrometer at a frequency of 400.13 MHz. Chemical shifts (δ) are given in ppm relative to the external standard tetramethylsilane.

The elemental analysis was carried out on an Elementar vario MACRO cube CHNS analyzer (Elementar Analysen system GmbH, Germany).

Initial substances and reactants

The initial reagents were prepared and experiments performed in an inert atmosphere (nitrogen) using a standard Schlenk flask and a glove box.

The solvents acetonitrile (Khimmed, reagent-grade), DMF (Ekos-1, reagent-grade), isopropanol (Ekos-1, reagent-grade), DMSO (Ekos-1, reagent-grade), chloroform (Komponent-reaktiv, reagent -grade), and THF (Ekos-1, reagent-grade) were absolutized using standard techniques [22] and stored under nitrogen atmosphere. Ethanol (95%) was used as-prepared.

Commercial reagents oleum (reagent-grade, 65% SO_3), HNO_3 (reagent-grade), NaOH (purum grade), HCl (reagent-grade), N_2H_4 H_2O (Vekton, imported), Bu_4NBF_4 (Alfa Aesar, 98%), $NiBr_2$ (Sigma Aldrich, 98%), isopentyl nitrite (Sigma Aldrich, 98%) and 1,10-phenanthroline monohydrate (Sigma Aldrich, 99%) were used as-prepared. The [$NiBr_2$phen] complex was prepared according to [23]. The technique employed in the present work for the preparation of BP and its characterization were described in [24]. The supporting electrolyte salt Bu_4NBF_4 was melted in a vacuum to remove residual water traces immediately before use.

Synthesis techniques

Synthesis of 5-nitro-1,10-phenanthroline. The synthesis was carried out according to Smith's procedure [25]. 1,10-Phenanthroline monohydrate (5 g, 25.25 mmol) was dissolved in 25% oleum (25 mL) in a 250 mL three-neck flask equipped with a thermometer and a magnetic stirrer. Concentrated nitric acid (13.3 mL) was added dropwise to the resulting solution, while maintaining the temperature of the mixture at ~165 °C and not exceeding 170 °C. After adding HNO_3, the solution was stirred for another 30 min. Then the reaction mixture was carefully poured into a glass of crushed ice (340 g). After the ice melted, the solution was neutralized by a 30% NaOH solution. A lilac color precipitate was formed for the solution with pH ≈3. The precipitate was filtered, dissolved in a dilute HCl solution, and then the solution was made alkaline using 30% NaOH. The resulting white precipitate of 5-nitro-1,10-phenanthroline was recrystallized from 95% ethanol (Scheme 1). Yield: 3.50 g (62%).

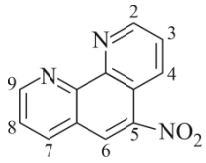

Scheme 1. Structure of 5-nitro-1,10-phenanthroline.

T_m = 197 °C. ^{1}H NMR (400 MHz, DMSO-d_6, 293 K): δ (ppm) 7.95 (m, 2H, C3–H, C8–H), 8.78 (dd, 1H, $^1J_{HH}$ = 8.07 Hz, $^2J_{HH}$ = 1.70 Hz, C7–H), 8.89 (dd, 1H, $^1J_{HH}$ = 8.58 Hz, $^2J_{HH}$ = 1.62 Hz, C4–H), 9.04 (s, 1H, C6–H), 9.25 (dd, 1H, $^1J_{HH}$ = 4.27 Hz, $^2J_{HH}$ = 1.60 Hz, C9–H), 9.29 (dd, 1H, $^1J_{HH}$ = 4.32 Hz, $^2J_{HH}$ = 1.82 Hz, C2–H). Elemental analysis: calculated (%) for $C_{12}H_7N_3O_2$: C 64.00, H 3.13, N 18.66. Found (%): C 65.30, H 3.02, N 18.25.

Synthesis of 5-amino-1,10-phenanthroline. The 10% Pd/C catalyst (60 mg) was added to a solution of 5-nitro-1,10-phenanthroline (425 mg, 1.89 mmol) in 95% ethanol (120 mL). A solution of $N_2H_4{\cdot}H_2O$ (1 mL) in ethanol (10 mL) was added dropwise to the obtained mixture. The reaction mixture was then boiled under reflux for 2 h. After completing the reaction, the hot solution was filtered from the catalyst, the solution was concentrated under vacuum to ~10 mL, and then the flask was left in a freezer to crystallize the product. The resulting precipitate was recrystallized from chloroform. Yield: 276 mg (75%).

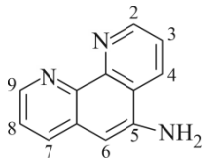

Scheme 2. Structure of 5-amino-1,10-phenanthroline.

T_m = 252 °C. ^{1}H NMR (400 MHz, DMSO-d_6, 293 K): δ (ppm) 6.12 (s, 2H, NH_2), 6.87 (s, 1H, C6–H), 7.51 (dd, 1H, C8–H), 7.74 (dd, 1H, C3–H), 8.05 (dd, 1H, C7–H), 8.68 (m, 2H, C4–H and C2–H), 9.06 (dd, 1H, C9–H). Elemental analysis: calculated (%) for $C_{12}H_9N_3$: C 73.83, H 4.65, N 21.52. Found (%): C 72.71, H 5.32, N 20.15.

Preparation of FLBP. FLBP was prepared by the electrochemical exfoliation of BP. To this aim, a solution of Bu_4NBF_4 (0.01 M) in DMSO (15 mL) was prepared in a 100 mL Schlenk flask. A BP cathode was placed in this solution the way that the BP clamp did not touch the solution. The anode was a Pt wire placed in the solution at a distance of ~1.5 cm from the BP. The electrodes were then connected to a power source, and the applied voltage was gradually increased from 1 V to 5 V within 5 min. Then the voltage was increased up to 10 V and maintained for 20 min. During the electrolysis, the electrode swelled significantly and gaseous products were released. After completing the exfoliation process, the swollen electrode was placed into a Schlenk flask with 5 mL of acetonitrile, and then the resulting mixture was sonicated for 1-2 min to remove the exfoliated FLBP from the BP surface. The obtained FLBP suspension was centrifuged at 9000 rpm, the precipitate was redispersed in a new portion of acetonitrile. This procedure was repeated several times to purify the FLBP. Finally, the FLBP was redispersed in THF, placed in a Schlenk flask and dried under vacuum. Solid FLBP was stored under nitrogen atmosphere.

Synthesis of FLBP–phen. The FLBP (10 mg) prepared by electrochemical exfoliation of BP was added into a solution of 5-amino-1,10-phenanthroline (97.5 mg, 0.5 mmol) in DMF (15 mL). The mixture was dispersed by sonication for 1 h and followed by the addition of isopentyl nitrite (0.13 mL, 1 mmol). The resulting suspension was heated to 80 °C and stirred at this temperature for 8 h. The functionalized FLBP particles were washed with DMF and several times with acetonitrile using successive centrifugation–decantation–redispersion procedure, placed into a Schlenk flask, and dried in a vacuum.

Preparation of FLBP–phen$NiBr_2$. $NiBr_2$ (25 mg, 0.11 mmol) was dissolved in DMF (5 mL). FLBP–phen (5 mg) was added to the obtained solution. Then the mixture was dispersed by 6 h sonication and stirred for 18 h. The functionalized FLBP particles were washed with DMF and several times by acetonitrile using successive centrifugation–decantation–redispersion procedure, placed into a Schlenk flask, and dried in a vacuum.

RESULTS AND DISCUSSION

The functionalization of FLBP was performed using an approach based on the in situ generation of a diazonium salt and subsequent reaction with FLBP obtained by the BP exfoliation by adding isopentyl nitrite to the mixture of FLBP and the amino derivative of 1,10-phenanthroline (Scheme 3). This approach was earlier successfully used for the functionalization of carbon nanotubes with various nitrogen-containing heterocyclic compounds [26].

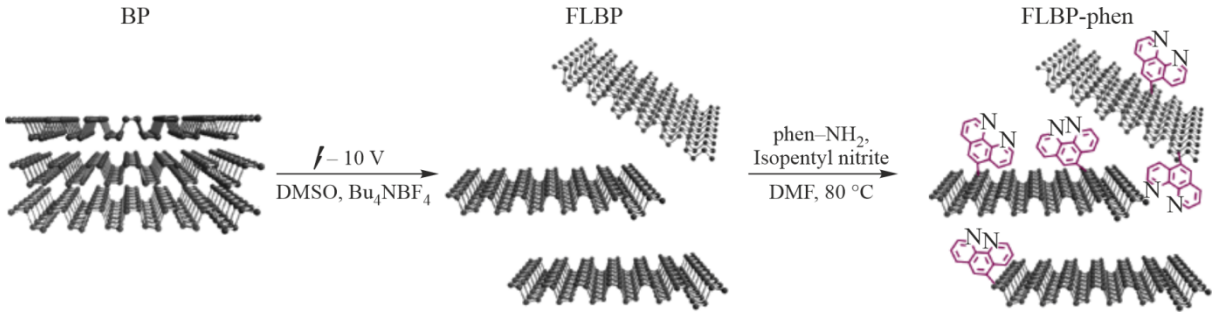

Scheme 3. FLBP functionalization with a phen-NH_2 amino derivative.

The 1,10-phenanthroline amino derivative (namely, 5-amino-1,10-phenanthroline (phen-NH_2)) was prepared according to the two-step synthesis shown in Scheme 4. First, phen was converted into 5-nitro-1,10-phenanthroline (phen-NO_2) by a nitration reaction using nitric acid and oleum. Then the nitro group of the resulting product was transformed into an amino group by reducing phen-NO_2 by hydrazine in the presence of the Pd/C catalyst. The formation of phen-NO_2 and phen-NH_2 products was confirmed by ^{1}H NMR spectroscopy.

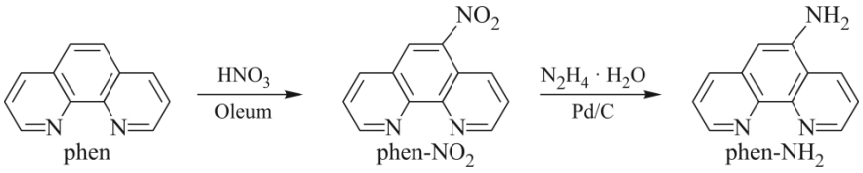

Scheme 4. Preparation of phen-NH_2.

The FLBP functionalization was carried out by adding isopentyl nitrite to a mixture of phen-NH_2 and electrochemically prepared FLBP in DMF and stirring the suspension for 8 h at 80 °C (Scheme 3). The FLBP–phen particles obtained after the functionalization were washed with DMF and acetonitrile and then dried in a vacuum. The isolated material was characterized by microscopic and spectroscopic methods.

The thickness and size of FLBP–phen particles were determined by TEM and AFM. Fig. 2 shows the AFM and TEM images of functionalized FLBP. The analysis of the obtained data showed that the exfoliation process led to the formation of FLBP particles with a width of 0.5-1.0 μm and a height of 8-10 nm. The TEM method also showed that the surface morphology of a small number of particles changed (became amorphous) as a result of functionalization. Amorphization of the surface is a side process of FLBP functionalization by diazonium salts, as was mentioned earlier in [9, 27, 28].

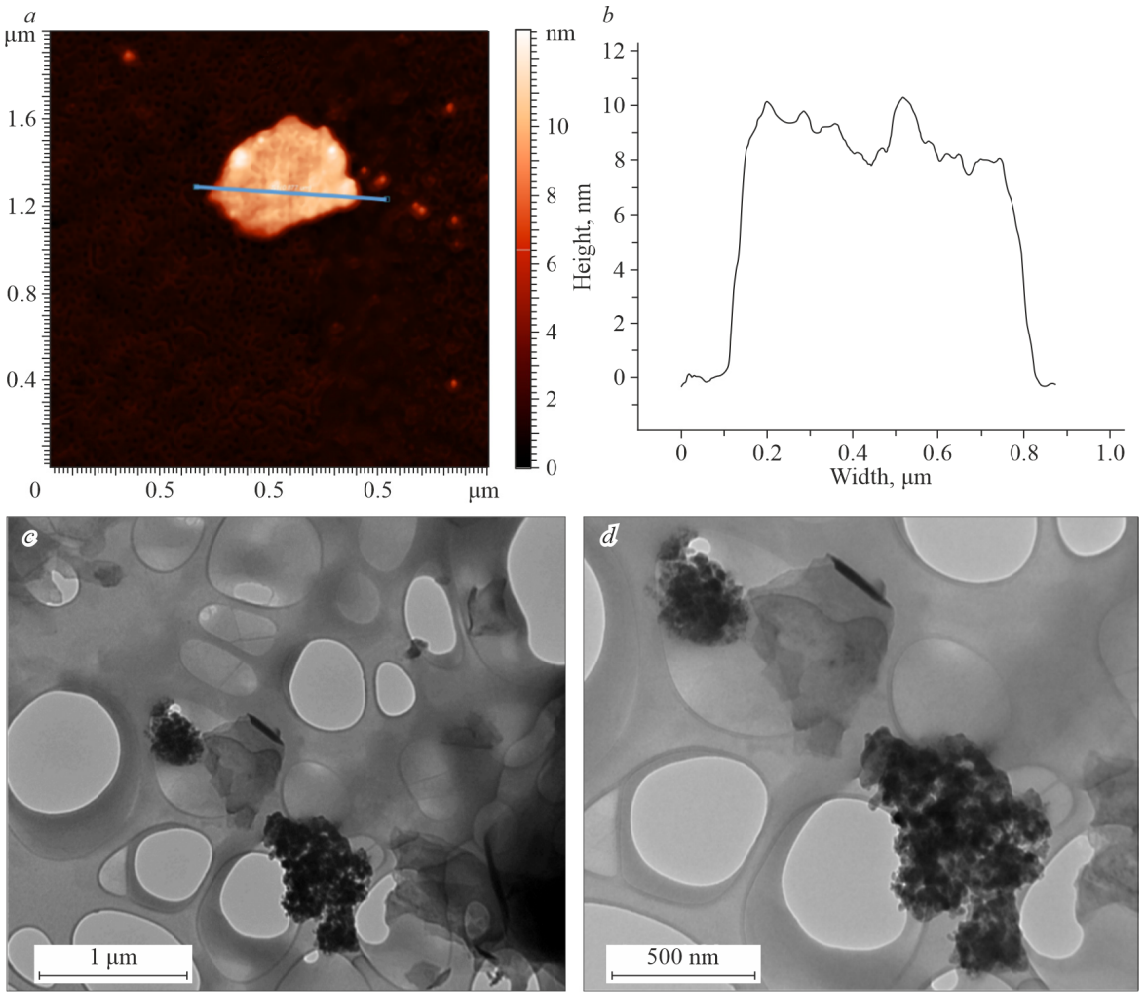

Fig. 2. AFM image of the surface of an FLBP-phen particle deposited on a SiO_2/Si substrate (*a*) and its cross section (*b*); TEM images of FLBP-phen particles deposited on a Lacey carbon substrate (*c*, *d*).

Fig. 3 shows the solid-state magic-angle spinning $^{31}P\{^{1}H\}$ NMR spectra (MAS NMR) for the FLBP–phen sample. According to the obtained data, the FLBP–phen sample contains, in addition to the main BP signal at 17.37 ppm, a wide shoulder from 10 ppm to –30 ppm, corresponding to the summed signals of new BP products formed during the functionalization [12, 14, 15, 29]. The obtained reaction products were studied in more detail by registering the spectrum in the $^{1}H - ^{31}P$ cross polarization magic-angle spinning (CP MAS) mode. Thus, the $^{1}H \rightarrow ^{31}P$ CP MAS NMR spectrum of the FLBP–phen sample shows a broadened signal with peaks at 2.8 ppm and –9.5 ppm. In this case, signals in the positive part of the spectrum are assigned to various forms of phosphorus-containing acids formed due to the partial oxidation of the FLBP surface [30], whereas the signal at –9.5 ppm indicates the appearance of a P–C bond in the sample and, therefore, covalent FLBP functionalization [12, 13, 29, 31].

The functionalized FLBP particles were also studied by the UV-vis spectroscopy (Fig. 4). Thus, the absorption spectrum of the FLBP–phen suspension in acetonitrile contains bands at 220 nm and 274 nm, corresponding to the absorption bands of 1,10-phenanthroline.

The Raman spectrum of FLBP–phen (Fig. 5) shows signals at 357.2 cm^{-1}, 431.6 cm^{-1}, and 459.7 cm^{-1} assigned to the A_g^1, B_{2g} and A_g^2 phonon modes of BP, respectively [32]. The spectrum also contains broadened peaks at 1032-1192 cm^{-1}, 1260-1333 cm^{-1}, and 1437-1569 cm^{-1} assigned to the phen molecules on the surface of the sample. Some shift of these

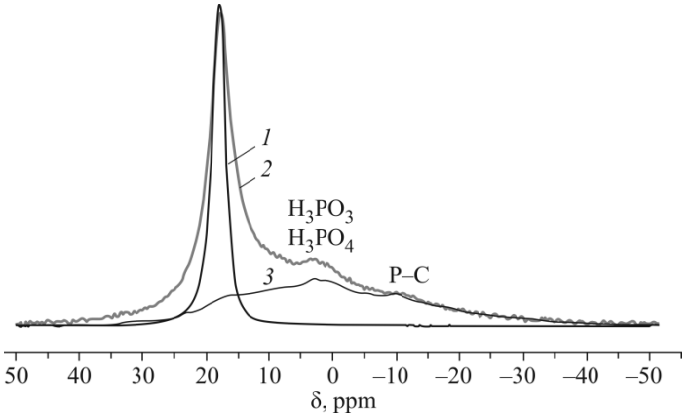

Fig. 3. ^{31}P MAS NMR spectrum of BP (*1*) and FLBP-phen (*2*) samples and $^{1}H \rightarrow ^{31}P$ CP MAS NMR spectrum of the FLBP-phen sample (*3*).

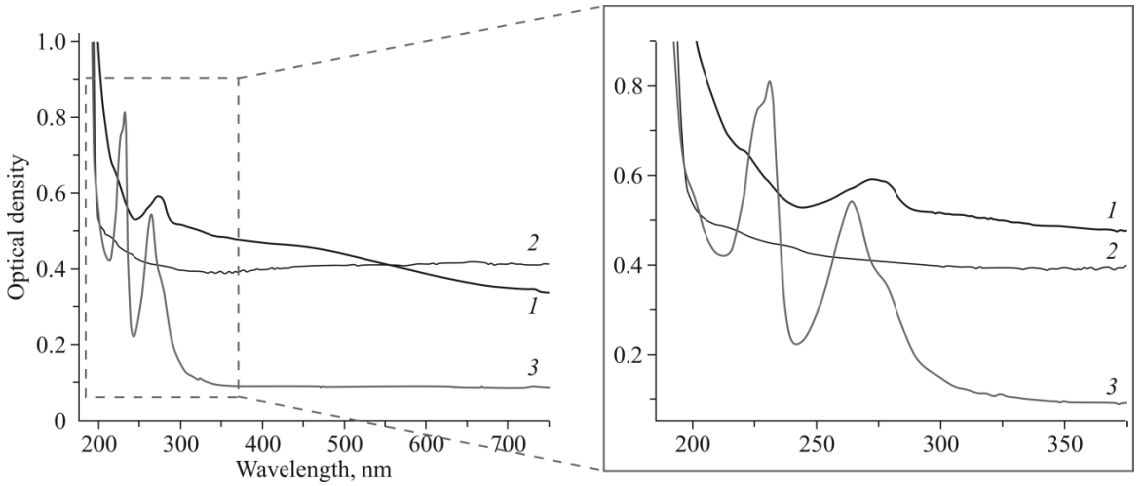

Fig. 4. Absorption spectra of FLBP-phen (*1*), FLBP (*2*), and phen (*3*). Magnified spectra in the 190-375 nm region (inset).

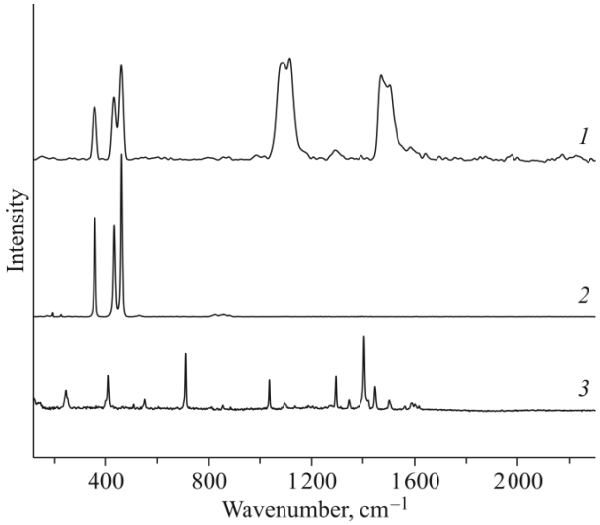

Fig. 5. Raman spectra for FLBP-phen (*1*), BP (*2*) and phen (*3*).

signals relative to those of pure phen may be due to the change in the structure of 1,10-phenanthroline as it is bonded to the phosphorus atoms in FLBP.

The FLBP–phen$NiBr_2$ particles were prepared by stirring FLBP–phen and $NiBr_2$ in DMF for 24 h (Scheme 5). The product was washed with DMF and several portions of acetonitrile and dried in a vacuum.

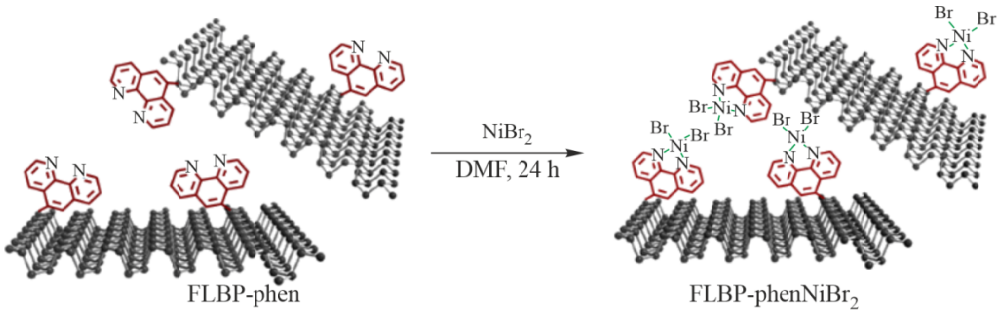

Scheme 5. Preparation of FLBP–phen$NiBr_2$.

The prepared material was characterized by various spectroscopic methods. The electron absorption spectrum of the FLBP–phen$NiBr_2$ suspension clearly shows a set of peaks at 239-269 nm corresponding to the [$NiBr_2$(phen)] bands (Fig. 6), thus indicating the formation of the [$NiBr_2$(phen)] complex on the FLBP surface. Moreover, the absence of a band at 274 nm for FLBP–phen$NiBr_2$ compared to the FLBP–phen spectrum indicates that the phen fragments on the FLBP surface are completely bound into the [$NiBr_2$(phen)] complex.

The Raman and IR spectra of FLBP–phen$NiBr_2$ also show signals corresponding to the vibrations of the [$NiBr_2$(phen)] complex. In addition to the signals in the region of 950-1270 cm^{-1} assigned to various types of P–O and P=O vibrations [33], the IR spectrum of FLBP–phen$NiBr_2$ (Fig. 7*a*) show also peaks at 796 cm^{-1}, 1350-1497 cm^{-1}, 1560-1740 cm^{-1}, and 2846-2963 cm^{-1}, indicating a presence of the [$NiBr_2$(phen)] complex on the material surface. The Raman spectrum of FLBP–phen$NiBr_2$ (Fig. 7*b*) is very much similar to that of FLBP–phen, except for a broadened peak at 780-920 cm^{-1}. Note however that the Raman spectrum of [$NiBr_2$(phen)] is very similar to that of the phen ligand, so it is difficult to confirm the formation of FLBP–phen$NiBr_2$ in the sample by this method.

The content of the nickel complex in the FLBP–phen$NiBr_2$ sample was determined by the energy dispersive X-ray spectroscopy (EDS) method. The EDS spectrum of the FLBP–phen$NiBr_2$ sample (Fig. 8) clearly shows the bands of nitrogen

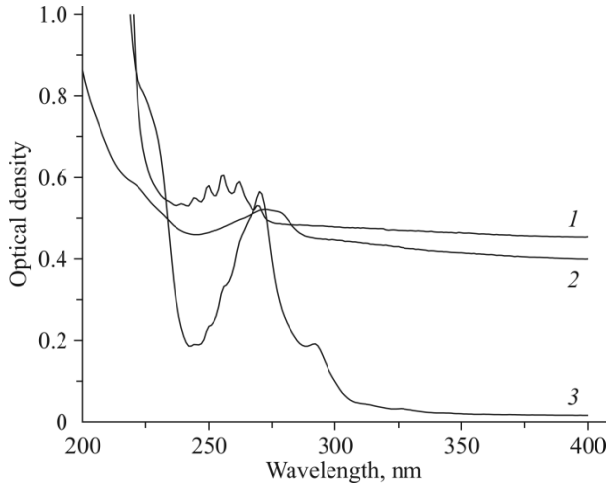

Fig. 6. Absorption spectra of FLBP-phenNiBr$_2$ (*1*), FLBP-phen (*2*), and [NiBr$_2$(phen)] (*3*).

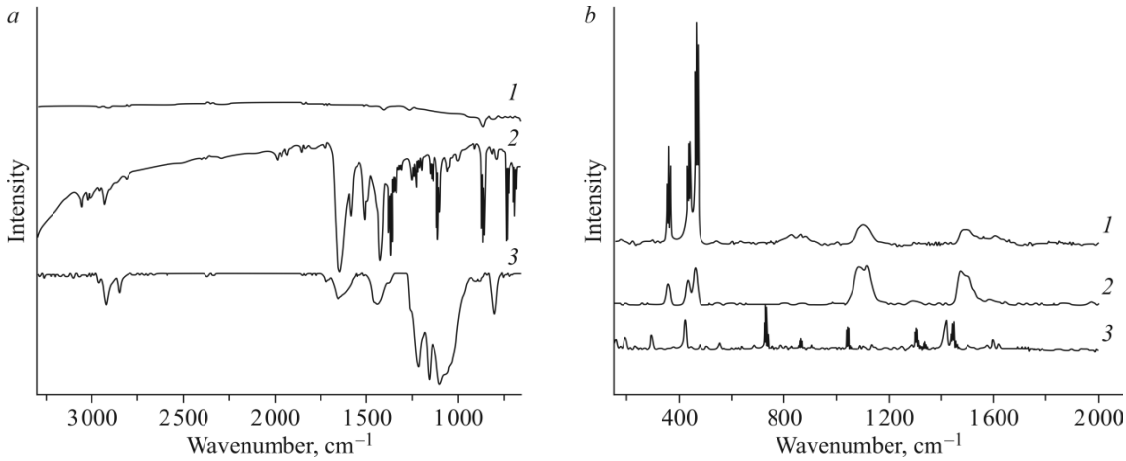

Fig. 7. IR spectra of FLBP (*1*), [NiBr$_2$(phen)] (*2*), and FLBP-phenNiBr$_2$ (*3*) (*a*); Raman spectra of FLBP-phenNiBr$_2$ (*1*), FLBP-phen (*2*), and [NiBr$_2$(phen)] (*3*) (*b*).

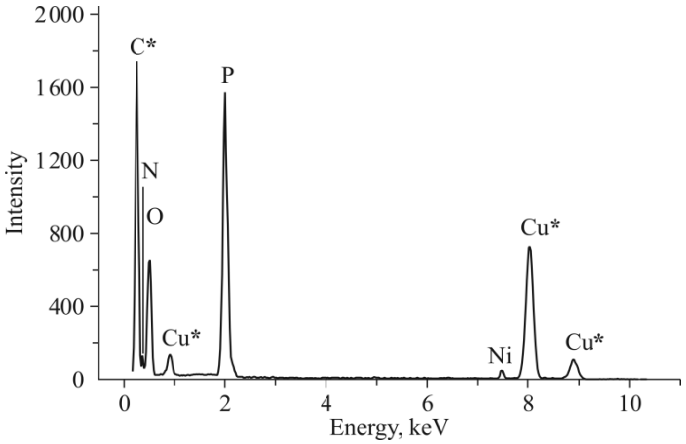

Fig. 8. EDS spectrum of FLBP–phenNiBr$_2$. The * symbol indicates the substrate signals.

($K_{\alpha 1}$ = 0.392 keV), oxygen ($K_{\alpha 1}$ = 0.525 keV), phosphorus ($K_{\alpha 1}$ = 2.013 keV), and nickel ($K_{\alpha 1}$ = 7.471 keV). The ratio of integral intensities of P and Ni showed that the Ni content in the sample was ~1%.

CONCLUSIONS

The immobilization of the [$NiBr_2$(phen)] complex on the FLBP surface was performed by covalent functionalization of FLBP by 1,10-phenanthroline (phen) and subsequent coordination of the latter to the $NiBr_2$ salt. The formation of the complex on the material surface was confirmed by electron absorption spectroscopy, solid-state NMR, energy-dispersive X-ray spectroscopy, Raman spectroscopy, and IR spectroscopy. The technique of immobilizing transition metal complexes on the FLBP surface can be used to create new types of heterogeneous catalytic systems with the possibility to regenerate the metal complex catalyst, as well as in various microelectronics devices and in biomedicine.

FUNDING

This work is financially supported by the Russian Science Foundation (project No. 23-13-00427). The solid-state NMR spectroscopy experiments were performed by O. I. Gnezdilov within the "PRIORITY-2030" development program of the Kazan Federal University.

CONFLICT OF INTERESTS

The authors of this work declare that they have no conflicts of interest.

REFERENCES

1. H. Liu, A. T. Neal, Z. Zhu, Z. Luo, X. Xu, D. Tománek, and P. D. Ye. Phosphorene: An unexplored 2d semiconductor with a high hole mobility. *ACS Nano*, **2014**, *8*(4), 4033-4041. https://doi.org/10.1021/nn501226z
2. S. C. Dhanabalan, J. S. Ponraj, Z. Guo, S. Li, Q. Bao, and H. Zhang. Emerging trends in phosphorene fabrication towards next generation devices. *Adv. Sci.*, **2017**, *4*(6). https://doi.org/10.1002/advs.201600305
3. X. Ren, P. Lian, D. Xie, Y. Yang, Y. Mei, X. Huang, Z. Wang, and X. Yin. Properties, preparation and application of black phosphorus/phosphorene for energy storage: a review. *J. Mater. Sci.*, **2017**, *52*(17), 10364-10386. https://doi.org/10.1007/s10853-017-1194-3
4. S. Bagheri, N. Mansouri, and E. Aghaie. Phosphorene: A new competitor for graphene. *Int. J. Hydrogen Energy*, **2016**, *41*(7), 4085-4095. https://doi.org/10.1016/j.ijhydene.2016.01.034
5. M. Luo, T. Fan, Y. Zhou, H. Zhang, and L. Mei. 2D black phosphorus–based biomedical applications. *Adv. Funct. Mater.*, **2019**, *29*(13). https://doi.org/10.1002/adfm.201808306
6. Y. Liu, M. Chen, and S. Yang. Chemical functionalization of 2D black phosphorus. *InfoMat*, **2021**, *3*(3), 231-251. https://doi.org/10.1002/inf2.12171
7. A. M. Kuchkaev, S. Lavate, A. M. Kuchkaev, A. V. Sukhov, R. Srivastava, and D. G. Yakhvarov. Chemical functionalization of 2D black phosphorus toward its applications in energy devices and catalysis: A review. *Energy Technol.*, **2021**, *9*(12). https://doi.org/10.1002/ente.202100581
8. S. Thurakkal and X. Zhang. Recent advances in chemical functionalization of 2D black phosphorous nanosheets. *Adv. Sci.*, **2020**, *7*(2). https://doi.org/10.1002/advs.201902359
9. C. R. Ryder, J. D. Wood, S. A. Wells, Y. Yang, D. Jariwala, T. J. Marks, G. C. Schatz, and M. C. Hersam. Covalent functionalization and passivation of exfoliated black phosphorus *via* aryl diazonium chemistry. *Nat. Chem.*, **2016**, *8*(6), 597-602. https://doi.org/10.1038/nchem.2505
10. M. van Druenen, F. Davitt, T. Collins, C. Glynn, C. O′Dwyer, J. D. Holmes, and G. Collins. Covalent functionalization of few-layer black phosphorus using iodonium salts and comparison to diazonium modified black phosphorus. *Chem. Mater.*, **2018**, *30*(14), 4667-4674. https://doi.org/10.1021/acs.chemmater.8b01306

11. S. Wild, M. Fickert, A. Mitrovic, V. Lloret, C. Neiss, J. A. Vidal-Moya, M. Á. Rivero-Crespo, A. Leyva-Pérez, K. Werbach, H. Peterlik, M. Grabau, H. Wittkämper, C. Papp, H. Steinrück, T. Pichler, A. Görling, F. Hauke, G. Abellán, and A. Hirsch. Lattice opening upon bulk reductive covalent functionalization of black phosphorus. *Angew. Chem., Int. Ed.*, **2019**, *58*(17), 5763-5768. https://doi.org/10.1002/anie.201811181
12. A. M. Kuchkaev, A. M. Kuchkaev, A. V. Sukhov, S. V. Saparina, O. I. Gnezdilov, A. E. Klimovitskii, S. A. Ziganshina, I. R. Nizameev, I. P. Asanov, K. A. Brylev, O. G. Sinyashin, and D. G. Yakhvarov. In-situ electrochemical exfoliation and methylation of black phosphorus into functionalized phosphorene nanosheets. *Int. J. Mol. Sci.*, **2023**, *24*(4), 3095. https://doi.org/10.3390/ijms24043095
13. A. M. Kuchkaev, A. M. Kuchkaev, A. V. Sukhov, S. V. Saparina, O. I. Gnezdilov, A. E. Klimovitskii, S. A. Ziganshina, I. R. Nizameev, I. R. Vakhitov, A. B. Dobrynin, D. I. Stoikov, G. A. Evtugyn, O. G. Sinyashin, X. Kang, and D. G. Yakhvarov. Covalent functionalization of black phosphorus nanosheets with dichlorocarbenes for enhanced electrocatalytic hydrogen evolution reaction. *Nanomaterials*, **2023**, *13*(5), 826. https://doi.org/10.3390/nano13050826
14. Y. Liu, P. Gao, T. Zhang, X. Zhu, M. Zhang, M. Chen, P. Du, G. Wang, H. Ji, J. Yang, and S. Yang. Azide passivation of black phosphorus nanosheets: Covalent functionalization affords ambient stability enhancement. *Angew. Chem., Int. Ed.*, **2019**, *58*(5), 1479-1483. https://doi.org/10.1002/anie.201813218
15. K. L. Walz Mitra, C. H. Chang, M. P. Hanrahan, J. Yang, D. Tofan, W. M. Holden, N. Govind, G. T. Seidler, A. J. Rossini, and A. Velian. Surface functionalization of black phosphorus with nitrenes: Identification of P=N bonds by using isotopic labeling. *Angew. Chem., Int. Ed.*, **2021**, *60*(16), 9127-9134. https://doi.org/10.1002/anie.202016033
16. Y. Zhao, L. Tong, Z. Li, N. Yang, H. Fu, L. Wu, H. Cui, W. Zhou, J. Wang, H. Wang, P. K. Chu, and X.-F. Yu. Stable and multifunctional dye-modified black phosphorus nanosheets for near-infrared imaging-guided photothermal therapy. *Chem. Mater.*, **2017**, *29*(17), 7131-7139. https://doi.org/10.1021/acs.chemmater.7b01106
17. S. Thurakkal and X. Zhang. Covalent functionalization of two-dimensional black phosphorus nanosheets with porphyrins and their photophysical characterization. *Mater. Chem. Front.*, **2021**, *5*(6), 2824-2831. https://doi.org/10.1039/d0qm00997k
18. Y. Cao, X. Tian, J. Gu, B. Liu, B. Zhang, S. Song, F. Fan, and Y. Chen. Covalent functionalization of black phosphorus with conjugated polymer for information storage. *Angew. Chem*., *Int. Ed.*, **2018**, *57*(17), 4543-4548. https://doi.org/10.1002/anie.201712675
19. G. E. Bekmukhamedov, A. V. Sukhov, A. M. Kuchkaev, A. M. Kuchkaev, K. R. Khayarov, A. B. Dobrynin, V. M. Babaev, and D. G. Yakhvarov. Catalytic performance of nickel(II) complexes bearing 1,10-phenanthroline based ligands in homogeneous ethylene oligomerization. *Polyhedron*, **2022**, *223*, 115978. https://doi.org/10.1016/j.poly.2022.115978
20. G. E. Bekmukhamedov, A. V. Sukhov, A. M. Kuchkaev, and D. G. Yakhvarov. Ni-based complexes in selective ethylene oligomerization processes. *Catalysts*, **2020**, *10*(5), 498. https://doi.org/10.3390/catal10050498
21. Z. N. Gafurov, I. F. Sakhapov, A. A. Kagilev, A. O. Kantyukov, I. K. Mikhailov, G. R. Ganeev, R. R. Faizullin, K. R. Khayarov, A. V. Gerasimov, and D. G. Yakhvarov. Synthesis, structure, and properties of the organonickel σ-complex [NiBr(Pmp)(bpy)], where Pmp is 2,3,4,5,6-pentamethylphenyl, bpy is 2,2′-bipyridine. *J. Struct. Chem.*, **2023**, *64*(1), 121-130. https://doi.org/10.1134/s0022476623010080
22. W. L. F. Armarego. Purification of Laboratory Chemicals, 8th ed. Butterworth-Heinemann Elsevier, **2017**.
23. M. Bialek, H. Cramail, A. Deffieux, and S. M. Guillaume. Styrene polymerization using nickel(II) complexes as catalysts. *Eur. Polym. J.*, **2005**, *41*(11), 2678-2684. https://doi.org/10.1016/j.eurpolymj.2005.05.024
24. A. M. Kuchkaev, A. V. Sukhov, A. M. Kuchkaev, S. A. Ziganshina, V. M. Babaev, A. T. Gubaidullin, A. B. Dobrynin, I. R. Nizameev, R. Shrivastava, S. Lavate, O. G. Sinyashin, and D. G. Yakhvarov. Electrochemical properties of nickel(II) ions in the presence of few-layer black phosphorus. *Russ. J. Electrochem.*, **2022**, *58*(8), 680-688. https://doi.org/10.1134/s1023193522080080.

25. G. F. Smith and F. W. Cagle. The improved synthesis of 5-nitro-1,10-phenanthroline. *J. Org. Chem.*, **1947**, *12*(6), 781-784. https://doi.org/10.1021/jo01170a007
26. G. Tuci, C. Zafferoni, A. Rossin, A. Milella, L. Luconi, M. Innocenti, L. Truong Phuoc, C. Duong-Viet, C. Pham-Huu, and G. Giambastiani. Chemically functionalized carbon nanotubes with pyridine groups as easily tunable N-decorated nanomaterials for the oxygen reduction reaction in alkaline medium. *Chem. Mater.*, **2014**, *26*(11), 3460-3470. https://doi.org/10.1021/cm500805c
27. A. Mitrović, S. Wild, V. Lloret, M. Fickert, M. Assebban, B. G. Márkus, F. Simon, F. Hauke, G. Abellán, and A. Hirsch. Interface amorphization of two-dimensional black phosphorus upon treatment with diazonium salts. *Chem. - Eur. J.*, **2021**, *27*(10), 3361-3366. https://doi.org/10.1002/chem.202003584
28. Z. Sofer, J. Luxa, D. Bouša, D. Sedmidubský, P. Lazar, T. Hartman, H. Hardtdegen, and M. Pumera. The covalent functionalization of layered black phosphorus by nucleophilic reagents. *Angew. Chem*., *Int. Ed.*, **2017**, *56*(33), 9891-9896. https://doi.org/10.1002/anie.201705722
29. H. Hu, H. Gao, L. Gao, F. Li, N. Xu, X. Long, Y. Hu, J. Jin, and J. Ma. Covalent functionalization of black phosphorus nanoflakes by carbon free radicals for durable air and water stability. *Nanoscale*, **2018**, *10*(13), 5834-5839. https://doi.org/10.1039/c7nr06085h
30. J. Plutnar, Z. Sofer, and M. Pumera. Products of degradation of black phosphorus in protic solvents. *ACS Nano*, **2018**, *12*(8), 8390-8396. https://doi.org/10.1021/acsnano.8b03740
31. P. Qiu, C. Xu, N. Zhou, H. Chen, and F. Jiang. Metal-free black phosphorus nanosheets-decorated graphitic carbon nitride nanosheets with C–P bonds for excellent photocatalytic nitrogen fixation. *Appl. Catal*., *B*, **2018**, *221*, 27-35. https://doi.org/10.1016/j.apcatb.2017.09.010
32. A. Favron, E. Gaufrès, F. Fossard, A.-L. Phaneuf-L′Heureux, N. Y.-W. Tang, P. L. Lévesque, A. Loiseau, R. Leonelli, S. Francoeur, and R. Martel. Photooxidation and quantum confinement effects in exfoliated black phosphorus. *Nat. Mater.*, **2015**, *14*(8), 826-832. https://doi.org/10.1038/nmat4299
33. A. C. Chapman, D. A. Long, and D. T. L. Jones. Spectra of phosphorous compounds - II. *Spectrochim. Acta*, **1965**, *21*(4), 633-640. https://doi.org/10.1016/0371-1951(65)80019-4